Biogeochemistry (2022) 160:159–175
https://doi.org/10.1007/s10533-022-00946-4

Production of dissolved carbon and alkalinity during macroalgal wrack degradation on beaches: a mesocosm experiment with implications for blue carbon

Anita K. Perkins · Isaac R. Santos · Andrew L. Rose · Kai G. Schulz · Hans-Peter Grossart · Bradley D. Eyre · Brendan P. Kelaher · Joanne M. Oakes

Received: 24 September 2021 / Accepted: 28 May 2022 / Published online: 9 July 2022

Abstract Marine macroalgae are a key primary producer in coastal ecosystems, but are often overlooked in blue carbon inventories. Large quantities of macroalgal detritus deposit on beaches, but the fate of wrack carbon (C) is little understood. If most of the wrack carbon is respired back to CO_2, there would be no net carbon sequestration. However, if most of the wrack carbon is converted to bicarbonate (alkalinity) or refractory DOC, wrack deposition would represent net carbon sequestration if at least part of the metabolic products (e.g., reduced Fe and S) are permanently removed (i.e., long-term burial) and the DOC is not remineralised. To investigate the release of macroalgal C via porewater and its potential to contribute to C sequestration (blue carbon), we monitored the degradation of *Ecklonia radiata* in flow-through mesocosms simulating tidal flushing on sandy beaches. Over 60 days, 81% of added *E. radiata* organic matter (OM) decomposed. Per 1 mol of detritus C, the degradation produced 0.48 ± 0.34 mol C of dissolved organic carbon (DOC) (59%) and 0.25 ± 0.07 mol C of dissolved inorganic carbon (DIC) (31%) in porewater, and a small amount of CO_2 (0.3 ± 0.0 mol C; ca. 3%) which was emitted to the atmosphere. A significant amount of carbonate alkalinity was found in porewater, equating to 33% (0.27 ± 0.05 mol C) of the total degraded C. The degradation occurred in two phases. In the first phase (days 0–3), 27% of the OM degraded, releasing highly reactive DOC. In the

Responsible Editor: Marguerite A. Xenopoulos.

Supplementary Information The online version contains supplementary material available at https://doi.org/10.1007/s10533-022-00946-4.

A. K. Perkins · A. L. Rose · K. G. Schulz · B. D. Eyre · J. M. Oakes
Centre for Coastal Biogeochemistry, Faculty of Science and Engineering, Southern Cross University, Lismore, NSW, Australia
e-mail: joanne.oakes@scu.edu.au

A. K. Perkins · I. R. Santos · B. P. Kelaher
National Marine Science Centre, Faculty of Science and Engineering, Southern Cross University, Coffs Harbour, NSW, Australia

A. K. Perkins · A. L. Rose · K. G. Schulz
Southern Cross Geoscience, Faculty of Science and Engineering, Southern Cross University, Lismore, NSW, Australia

I. R. Santos
Department of Marine Sciences, University of Gothenburg, Göteborg, Sweden

H.-P. Grossart (✉)
Leibniz Institute for Freshwater Ecology and Inland Fisheries (IGB), Experimental Limnology, Neuglobsow, Germany
e-mail: hanspeter.grossart@igb-berlin.de

H.-P. Grossart
Institute of Biochemistry and Biology, University of Potsdam, Potsdam, Germany

second phase (days 4–60), the labile DOC was converted to DIC. The mechanisms underlying *E. radiata* degradation were sulphate reduction and ammonification. It is likely that the carbonate alkalinity was primarily produced through sulphate reduction. The formation of carbonate alkalinity and semi-labile or refractory DOC from beach wrack has the potential to play an overlooked role in coastal carbon cycling and contribute to marine carbon sequestration.

Graphical abstract

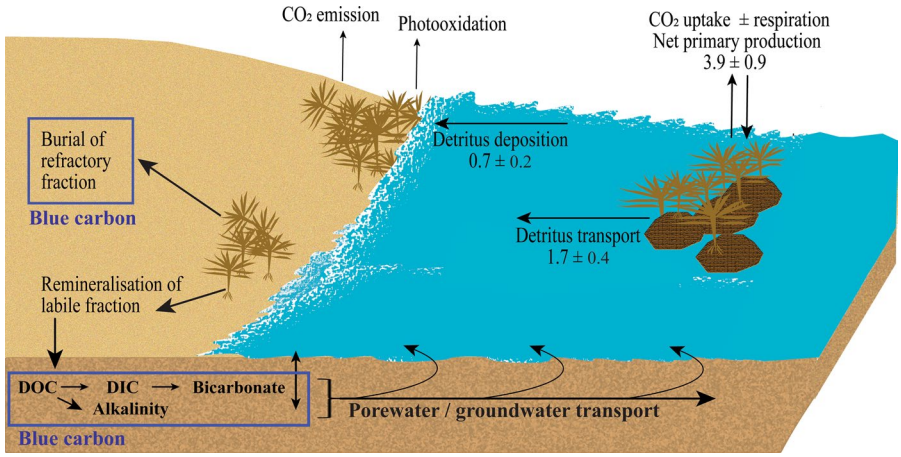

Keywords Tidal pumping · Organic matter degradation · Carbon cycle · Mineralisation · Porewater exchange · Submarine groundwater discharge

Introduction

Marine macroalgae are major primary producers in coastal waters (Säwström et al. 2016), covering up to 23% of global coastlines (Gattuso et al. 2006), and contributing an estimated 1521 Tg C yr^{-1} of net primary production (NPP) (1020–1960 Tg C yr^{-1}) (Krause-Jensen and Duarte 2016). Primary production by marine macroalgae exceeds that from other coastal primary producers (Krause-Jensen and Duarte 2016). However, although other primary producers such as mangrove forests, saltmarshes and seagrass beds are recognised as important contributors to blue carbon (Duarte 2017; Krause-Jensen et al. 2018; Raven 2018; Filbee-Dexter and Wernberg 2020), remineralised before it can be buried (Krause-Jensen and Duarte 2016), which may limit their capacity to be a blue carbon sink. A first budget estimate suggests that 173 Tg C yr^{-1} is sequestered globally as macroalgae detritus (Krause-Jensen and Duarte 2016), but this calculation does not include the blue carbon potential from remineralisation of detritus on beaches (e.g., production of carbonate alkalinity). Macroalgal detritus is highly mobile; macroalgal senescence macroalgae are typically overlooked. This reflects the conventional understanding that coastal vegetation contributes blue carbon if its biomass is converted to permanently stored C. Macroalgae grow on hard substrates that preclude local C burial and storage. However, there is potential for macroalgae to contribute significant blue carbon through transport and storage in receiver environments (McLeod et al. 2011; Hill et al. 2015) or via degradation pathways that consume coastal carbon through, for example, calcium carbonate dissolution or carbonate alkalinity production.

Potentially, macroalgae are a larger blue carbon sink than seagrass beds, salt marshes, or mangrove forests. For example, macroalgae cover a larger area (Duarte 2017) and have a higher NPP (Alongi 2020) than traditional blue carbon habitats (seagras beds, salt marshes, or mangrove forests) and 82% of algal biomass enters the detrital pathway (Krumhansl and Scheibling 2012). However, macroalgae also tend to degrade faster than plants, with approximately 58% of macroalgal biomass rapidly

results in continuous export of detritus C through a highly variable 'decay voyage' (Kirkman and Kendrick 1997; Krumhansl and Scheibling 2012; Hill et al. 2015). During transport, the macroalgal C is partly remineralised in water, or on the coastal shelf, and is partly deposited in receiver habitats as long-term C storage (Krumhansl and Scheibling 2012; Hill et al. 2015; Krause-Jensen and Duarte 2016). A large portion of macroalgal C export is deposited on beaches, yet no carbon mass balance has been determined for sandy beaches. It also remains unclear what the degradation products are, how much C can contribute to other forms of blue carbon that could be as important as burial, and if the degrading products can enter porewater through the beach sediments, where it can be re-distributed to the marine environment.

The composition of macroalgal detritus and environmental conditions (e.g., temperature and available oxygen), influence the degradation and remineralisation pathways for macroalgal biomass (hereafter called wrack). The term 'degradation' relates to the fragmentation of organic matter (OM) into particulate organic carbon (POC) or its conversion to dissolved organic carbon (DOC) forms, and the term 'remineralisation' relates to the conversion of organic C to inorganic C. Thus, degradation of wrack C may be assimilated into new microbial biomass, POC, or DOC, and through remineralisation is converted into CO_2, CH_4, dissolved inorganic carbon (DIC) or alkalinity. These processing pathways may contribute to blue carbon or offset blue carbon. POC turns into DOC and the contribution to blue carbon is complex, as DOC can be labile, semi-labile, or refractory. The reactivity of DOC and the molecular weight of C compounds determine whether C is remineralised, or sequestered long-term (4–600 years) (Lechtenfeld et al. 2014; Santos et al. 2021). DIC is comprised of CO_2, bicarbonate and calcium carbonate and in the ocean can represent long-term storage for blue carbon (100,000 years) as bicarbonate.

The speciation of DIC is pH dependent. At high seawater pH, most DIC is present as alkalinity. If organic matter mineralisation produces alkalinity, the process could represent carbon storage in the ocean and a buffer against ocean acidification (Sippo et al. 2016; Saderne et al. 2020; Wagner et al. 2020) if at least part of the metabolic products (e.g., reduced Fe and S) are permanently removed (i.e., long-term burial). Full conversion of macroalgal biomass to CO_2 and CH_4, followed by its emission to the atmosphere, represents an offset to blue carbon (Rosentreter et al. 2018). C from the decomposing wrack on beaches may enter porewater in coastal areas, with porewater having the potential to transport solutes back to the ocean. Yet, the fate of processing pathways (DOC, DIC and alkalinity) of kelp detritus and the role of porewater in transporting the C from the decomposing macroalgae on beaches remains unexplored (Kelleway et al. 2017; Macreadie et al. 2019).

Here, we quantified the fate of macroalgal carbon and its major degradation pathways in a mesocosm experiment simulating a sandy beach. Macroalgal degradation was assessed over a 60-day incubation period. We used the southern hemisphere kelp *Ecklonia radiata*, which is the dominant macroalga in Australia's temperate reefs (Wernberg et al. 2003; Kelaher et al. 2013; Marzinelli et al. 2015). Around Australia, *E. radiata* represents ca. 10.3–22.7 Tg C biomass with ca. 1.3–2.8 Tg C yr^{-1} of potential carbon sequestration via the conventional detrital pathway (Filbee-Dexter and Wernberg 2020), but this proportion does not include the blue carbon potential from biomass remineralisation on beaches. We estimated C sources and sinks over the course of the degradation. The underlying biogeochemical processes of remineralisation were assessed by the stoichiometric ratios of TA and DIC. We hypothesised that (1) *E. radiata* biomass on sandy beaches is primarily converted to DOC, (2) part of the DOC is remineralised into DIC and carbonate alkalinity, and (3) the production of carbonate alkalinity from remineralisation of *E. radiata* biomass is an important contributor of blue carbon.

Methods

Experimental setup

To simulate a tidal beach environment under controlled conditions, we built eight individual beach simulator flow-through mesocosms, each constructed of a 10 cm diameter, 180 cm tall polyvinyl chloride (PVC) pipe (Fig. 1a, b). A pipe at the base of each mesocosm connected to a separate 2 cm diameter, 160 cm tall PVC pipe in an inverted 'U' shape, allowed control of the water level in the mesocosm to simulate the tidal cycle. To this second PVC pipe,

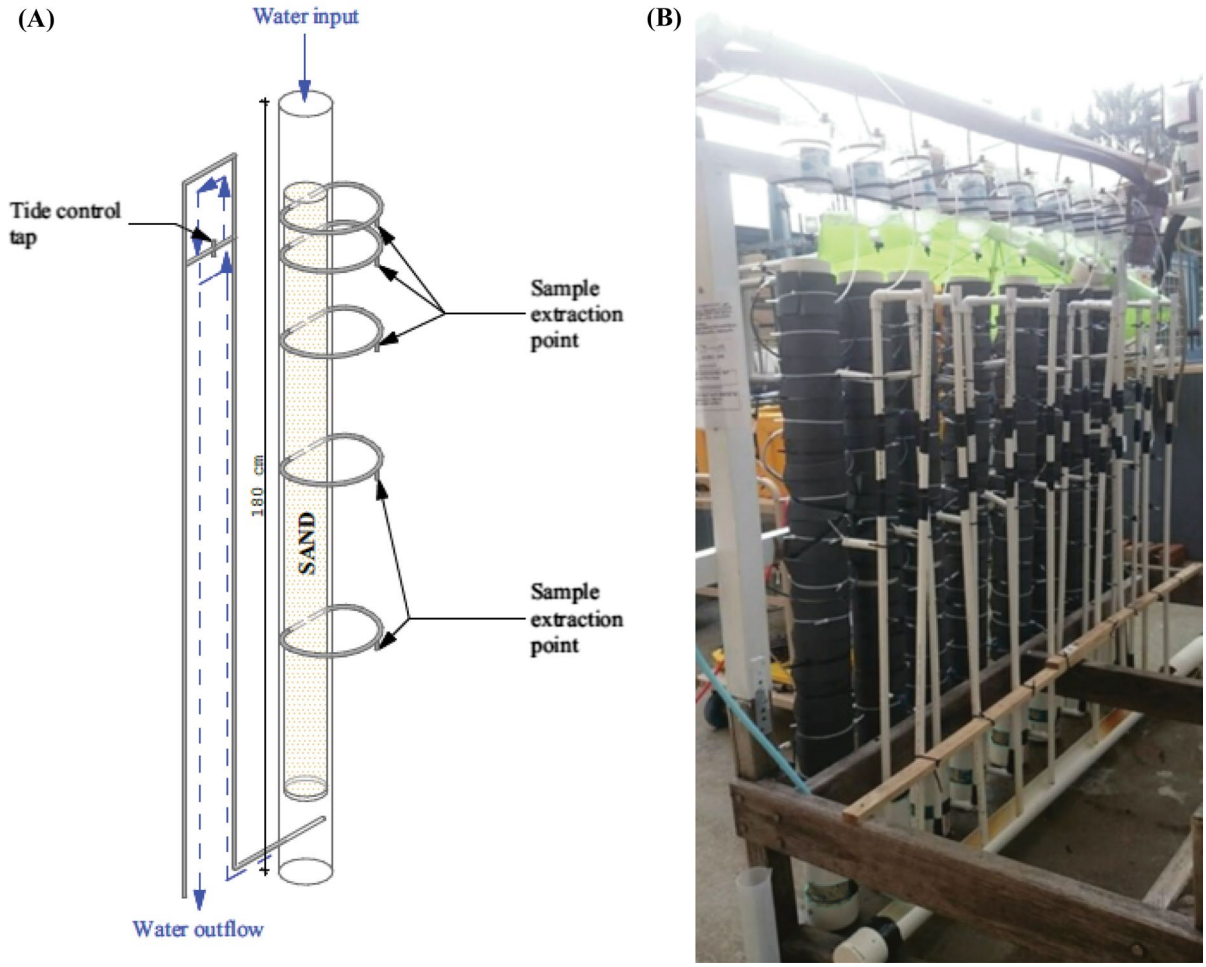

Fig. 1 Schematic diagram of beach simulator (mesocosm) (**A**) and photograph of the set up (**B**)

a 4 mm flexible tubing with 4 mm taps was connected to enable the water to be drained to a specific height to simulate each tide. Samplers consisting of a grid of punctured rigid irrigation tubing, each covered with a 38 µm mesh, were installed at 1, 10, 30, 60 and 100 cm below the surface of the sand in the mesocosm to enable collection of porewater from the entire cross-section of the mesocosms at each depth.

Surface sand [22.2% medium sand (250–500 µm), 73.2% fine sand (125–250 µm) and 4.5% very fine sand (63–125 µm)] was collected from Arrawarra Beach (NSW, Australia 30.059119S, 153.198414E) at low tide, sieved (500 µm) to remove beach cast OM, and homogenised. The carbonate content of the sediment was determined to be < 5% based on mass change following digestion with 25% HCl (MacCharthy 1933). Seawater was obtained directly from the sea through a flow-through seawater supply system. The seawater was filtered through a 5 µm sediment filter membrane (Stefani water filter, Bunnings Warehouse Australia). Each mesocosm was acid washed with 10% HCl for 24 h before the addition of the sand, and the homogenised sand was used to fill each mesocosm to a height of 120 cm. Mesocosms were then drip-fed with seawater for 2 weeks to allow sediment stabilisation before macroalgae wrack was added to begin the degradation experiment.

Fresh *E. radiata* was collected from Charlesworth Bay (30.267583S, 153.143741E), the holdfast was removed, and the remainder of the *E. radiata*

was then washed with tap water. To homogenise the *E. radiata* material, first it was semi-sun-dried over 2 days, then oven-dried to constant weight (60 °C, 72 h). After drying, the algal material was crushed to 0.5–2 cm sized fragments and stored at – 18 °C until the experiment commenced. Dried *E. radiata* fragments (200 g dry weight per mesocosm) were placed on top of the sand of four mesocosms, with the remaining four mesocosms serving as controls containing sand only.

Filtered seawater was used to fill tap-equipped 1.5 L polypropylene bottles, which acted as individual 'header tanks' that drip-fed each mesocosm. 1.5 L of seawater was drip-fed over 30 min into each mesocosm. The filtration ensured no external addition of phytoplankton biomass to the mesocosms so that the macroalgae remained the primary carbon source. The mesocosms were repeatedly inundated from the top with filtered seawater then drained to one centimetre beneath the surface of the sand, thereby simulating natural tidal cycles and the retention of porewater between high tides. The amount of water added was the same as that drained from the bottom of the mesocosms through the outflow. The drained water was disposed of, and fresh filtered seawater was used to inundate the mesocosms each time. In this way, only porewater would stay in the system, simulating a tidally driven porewater flow back to the ocean. Because macroalgae often accumulates in the tidal regions of beaches, each mesocosm was inundated twice daily (at 7 am and 7 pm) for 2 h each time to simulate high tide then drained for 10 h each time to simulate low tide. During 'high tide', seawater covered the wrack and during 'low tide', the water level remained below the wrack, at 1 cm beneath the surface of the sand. The beach simulator was maintained outdoors, under natural daylight conditions.

To estimate the change in detrital mass over time, nine 10 cm × 10 cm mesh bags (mesh size 38 µm), each containing 1 g of *E. radiata*, were placed in each of the four treatment mesocosms at the commencement of the experiment. One bag per mesocosm was sacrificed at each sampling time (0.5 day, 1 day, 3 days, 6 days, 10 days, 20 days, 30 days, 45 days and 60 days), then rinsed with tap water and oven dried to constant weight (60 °C, 72 h). The proportion of mass lost from the bag was then used to estimate the proportion of mass lost over time from the kelp wrack.

Porewater sampling and analysis

Following the period of inundation, samples were collected before drainage, ensuring that the water samples collected from each port reflected processes occurring at a known sediment depth. At each sampling time, 180 mL of porewater were drawn for analysis from each of the sampling ports. The sample water was collected from the full cross section of the mesocosms where punctured pipe threaded through the mesocosm allowed for drawing sample water from all angles. With 39% porosity, each pipe contained ~ 3.6 L of water, equating to 300 mL of water per 10 cm depth increment. Temperature, pH and dissolved oxygen (DO) were determined by a Hach multiprobe 40D. DO concentrations were measured immediately after draining the sample water to prevent oxygen contamination and ensuring the data gathered was a true reflection of sediment conditions. Sub-samples for DIC, DOC, nutrients, dissolved CO_2 and CH_4 from porewater (denoted as $CO_{2Porewater}$ and $CH_{4Porewater}$, respectively), and alkalinity were filtered through 0.7 µm GF/F syringe filters. From the porewater, DIC and DOC sub-samples were collected without a headspace into 40 mL borosilicate vials and treated with 100 µL of saturated $HgCl_2$ to inhibit any microbial activity and stored at 4 °C until analysis. DIC and DOC concentrations were measured with a TOC-V_{chp} Shimadzu total organic carbon (TOC) analyser (Jones and Willett 2006). TA samples were collected into 40 mL polypropylene vials, stored at 4 °C until analysis, then determined via potentiometric titration (Mos et al. 2021) with a Metrohm Titrino 848 Automatic Potentiometric Titrator. Prior to running the daily sample titrations, the titrator was run with seawater and in-house-standards (Dickson et al. 2003), which allowed for daily corrections to ensure accuracy. Sub-samples for NH_4^+ and PO_4^{3-} were collected in 10 mL polypropylene vials and stored at − 18 °C until analysis. Concentrations of NH_4^+ and PO_4^{3-} were determined via a Lachat QuickChem 8000 Flow Injection Analyser (FIA) with four channels (for details, detection limits, accuracy, precision and error, see McKee et al. 2000).

Dissolved $CO_{2Porewater}$ and $CH_{4Porewater}$ samples were collected in 40 mL borosilicate vials without headspace and treated with 100 µL saturated $HgCl_2$. A headspace was then created by injecting 20 mL of nitrogen gas while withdrawing 20 mL of the sample

water. Dissolved gases were equilibrated between the aqueous phase and headspace through agitation of the vials for 15 min at 180 rpm with an RM2 shaker. After agitation, the headspace gas was collected into a syringe and injected into a Picarro G2401 high precision gas analyser for analysis of $CO_{2Porewater}$ and $CH_{4Porewater}$ concentrations (as per Maher et al. 2013). To ensure the accuracy of the instrument, the Picarro was calibrated before and after the experiment.

Determination of CO_2 and CH_4 emissions

To capture the emission of CO_2 and CH_4 (denoted as $CO_{2Emission}$ and $CH_{4Emission}$, respectively) from the sediment to the overlying air during kelp degradation, a PVC pipe cover was modified to act as a 'cap' on top of the mesocosm. Two holes were drilled into the cap and 4 mm diameter gas tight tubing was inserted and secured with gas tight tape. On each sampling day, the tubes formed a closed circuit between the Picarro G2401 and the mesocosm to directly measure the emitted $CO_{2Emission}$ and $CH_{4Emission}$ in the headspace. Each mesocosm was 'capped' for 5 min while connected to the Picarro. Between samplings, the Picarro was allowed to re-equilibrate to atmospheric concentrations.

Flux and budget calculations

For visual interpretation over time and depth, the differences between all chemical parameters in treatment and control mesocosms were calculated for each time and depth (Eq. 1):

$$\Delta C = C_{Treatment} - C_{Control} \quad (1)$$

where ΔC (mmol/L) represents the average difference in concentrations of parameters between treatment and control, and $C_{\text{Treatment}}$ (mmol/L) and C_{Control} (mmol/L) represents the average concentration of a parameter across replicates for the four mesocosms containing detritus (treatment), and for the four control mesocosms, respectively. Secondly, we calculated the difference in flux (export) for each parameter (DOC, DIC CO_2, CH_4, TA, NH_4^+, PO_4^+) between treatment ($C_{\text{Treatment}}$) and control (C_{Control}) mesocosms, as follows (Eq. 2):

$$C_{Flux} = \left(C_{Treatment} \times V_{Tide}\right) - \left(C_{Control} \times V_{Tide}\right) \quad (2)$$

where C_{Flux} (mmol/d) represents the flux of material accounted for only by macroalgal detritus addition, V_{Tide} (L/d) represents the daily volume of seawater addition (diel tidal input) and $C_{\text{Treatment}}$ (mmol/L) and C_{Control} (mmol/L) are the average concentration of a parameter across replicates in treatment and control mesocosms, respectively. To calculate the rates of CO_2 and CH_4 emission (denoted as $CO_{2Emission}$ and $CH_{4Emission}$), the change in concentration over time (ppmv/min) was determined by linear regression of concentration against time for the first minute of measurements taken after concentrations started to rise. The emitted flux ($C_{\text{Emitted flux}}$ in mmol/day) was then calculated using Eq. 3:

$$C_{Emitted\,flux} = \Delta C_{Emission\,rate} \times D \times \frac{V_{Headspace}}{\mathrm{MW_{Gas}}} \times \frac{1440\mathrm{min}}{\mathrm{d}} \times \frac{1000\mathrm{mmol}}{\mathrm{mol}}, \quad (3)$$

where $\Delta C_{\text{Emission rate}}$ (ppmv/min) represents the difference in rates of emission per minute between treatment and control, D (g/L) represents the density of gases under standard temperature and pressure, $V_{\text{headspace}}$ (L) represents the volume of gas in the headspace (2.5 L), and $\mathrm{MW_{gas}}$ (g/mol) represents the molecular mass of the gas.

C_{Flux} and $C_{\text{Emitted flux}}$ were plotted against time for the experimental period. Assuming a linear rate of change in flux rates between sampling times, we interpolated between each data point to determine the area under the curve, which equated to the total amount (mmol) of C removed via each pathway between sampling times.

The mass balance can be calculated in two ways: (1) using the average measurements (treatment-control) for each parameter at each depth per treatment mesocosm, and (2) using only the average measurements (treatment-control) for parameters at 100 cm depth. The first of these approaches assumes that the export of degradation products from the beach occurs via lateral porewater flow; in this case the total export of degradation products equals the sum of degradation products across depths. In contrast, the second approach assumes that degradation products are transported downwards as they are processed within the sediment. The products found at 100 cm depth are then exported to the coastal ocean (Tables S1–S3). For the overall calculation of the mass balance, DOC

values were similar with either method, while DIC and alkalinity were higher at 100 cm depth. The total estimated C output (Tables S1 and S2) was closer to the used biomass estimate (wrack biomass loss estimated from 1 g bags) when values from a depth of 100 cm were used. Therefore, the second approach using values from a depth of 100 cm were used to determine the C budget. Theoretically, this would equate to the total carbon in the measured transformation and loss pathways, i.e., $DOC_{Porewater}$ (measured DOC in the porewater), $DIC_{Porewater}$ (DIC in the porewater including $CO_{2Porewater}$ and $CH_{4Porewater}$), $CO_{2Emission}$ (CO_2 emissions to the atmosphere), $CH_{4Emission}$ (CH_4^+ emissions to the atmosphere) and C_{Sand} (the change in organic carbon content in the sediment from before and after 60 days of degradation).

$$C_{E.radiata} = DOC_{Porewater} + DIC_{Porewater} + CO_{2Emission} + CH_{4Emission} + C_{Sand} \quad (4)$$

Our calculation focussed on the dissolved components and assumed that any POC would remain in the sediment column (C_{Sand}). Although there is potential for photo-oxidation to influence the degradation of exposed wrack, this would be limited to the surface of the wrack pile and would contribute little to the sediment processing that was the focus of this study. This pathway was therefore excluded from the mass budget. Furthermore, the input of macroalgal biomass released as nutrients may have, in turn, enhanced the growth of microalgae in the treatment mesocosm. However, we could also not account for this component.

Statistical analysis

The mass loss of detritus from 1 g bags was assessed using a mass decay plot to determine if the decay was best described by 1, 2 or 3 phases of degradation. This was determined using the Origin 2020 nonlinear exponential decay function. To further explore the maximum likelihood of the decay models (1, 2, or 3 phases), each model was compared with Akaike's Information Criterion (AIC) test and Bayesian Information Criterion (BIC) test. The mass decay model selected had lower AIC and BIC values (details are in the supplementary information, Table S5).

To test if macroalgae is a significant C-input to sandy shores, a t-test was performed for each measured variable ($DIC_{Porewater}$, $DOC_{Porewater}$, $TA_{Porewater}$, $NH_4^+{}_{Porewater}$, $PO_4^{3-}{}_{Porewater}$, $CO_{2Emission}$, $CH_{4Emission}$, pH and DO) (Table S4) using the averaged treatment versus the averaged control measurements from all depths and time points. The stoichiometric ratios of TA:DIC were assessed in a regression model to identify pathways based on known typical ratios for the different biogeochemical processes (e.g. aerobic respiration, denitrification, ammonification, sulphate reduction, calcium carbonate dissolution, manganese reduction, and iron reduction) (Borges et al. 2003).

To test hypothesis four, the two factors (time and sediment depth) were assessed to ascertain which factor was influencing the C values more. As the interaction between the two factors is strong (ANOVA $P = 1.6 \times 10^{-4}$), ANOSIM was used to test spatial and temporal variability. In ANOSIM, the factors can be crossed and nested (A:spatial variable of depth in the mesocosm, B:temporal variable of measured time point) (Somerfield et al. 2021) with the four replicates of all C variables ($DOC_{Porewater}$, $DIC_{Porewater}$, $TA_{Porewater}$, $CO_{2Porewater,}$ $CH_{4Porewater}$ over time and depth). C variables were ranked in a permutational ANOSIM (with Primer 7), where 'R' is the statistical parameter, to represent the strength of factors between time and depth. To visualise the effects of depth as a factor on all C components, the normalised C variables were ordinated with Bray–Curtis resemblances via non-metric multidimensional scaling (nMDS), and also with Primer 7 (Somerfield et al. 2021).

Results

Porewater chemical properties during kelp degradation

A change in porewater chemistry was evident following the addition of kelp to the mesocosms (Fig. 2). By day 1, DO concentrations decreased substantially (< 14% saturation) at all depths, and below 60 cm DO concentrations remained low throughout the 60 days of degradation (Fig. S1). The average pH under the degrading kelp wrack over time was typically one unit

Table 1 Mass balance of *E. radiata* C degradation for the total 200 g dry weight *E. radiata* OM (5978 mmol C) added to each mesocosm (details in Table S1 and S2)

	OM degraded	$DOC_{Porewater}$	$DIC_{Porewater}$	$CO_{2Emission}$	$CH_{4Emission}$	$TA_{Porewater}$
Used C	**4856**	**2880 ± 1992**	**1514 ± 437**	**157 ± 135**	**0.3 ± 0.44**	**1618 ± 158**
$C_{First\text{-}phase}$	1614	1787 ± 1764	33 ± 7	2 ± 1	$2\times10^{-4} \pm 4\times10^{-4}$	74 ± 18
$C_{Second\text{-}phase}$	3242	1093 ± 228	1481 ± 430	155 ± 134	0.3 ± 0.44	1544 ± 140

Of the added biomass, 4856 ± 60 mmol C was degraded (=total used C, or daily input from the 1 g bags). All units are in mmol (mean ± SE)

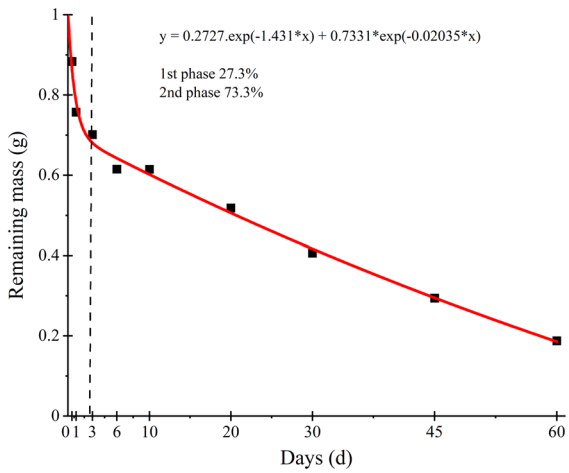

Fig. 2 Biomass C loss during E. radiata degradation over 60 days. The red line represents the line of best fit for the two-component exponential decay model and the dotted line separates the first and second phases of degradation

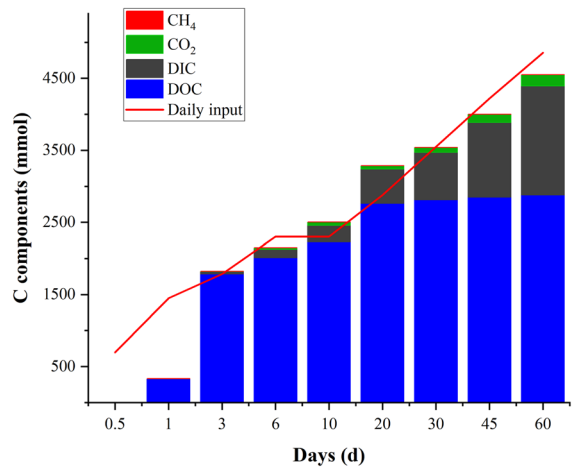

Fig. 3 The cumulative production of the main C components produced during E. radiata degradation. The daily input represents the mass loss from 1 g bags of detritus. DIC and DOC are from the sediment porewater and $CO_{2Emission}$ and $CH_{4Emission}$ are emissions to overlying air

lower than the control, with the lowest pH recorded on day six near the surface. pH and DO showed an inverse relationship, with the pH lower near the surface and increasing with depth, whereas DO was higher near the surface and decreased with depth and over time.

Macroalgal-C degradation

The addition of kelp wrack to each mesocosm was equivalent to 5978 mmol C per mesocosm. Throughout the whole experiment, concentrations of organic C in the sand in the treatment mesocosms were low (organic C content decreased from 0.038 to 0.027%). *E. radiata* detritus had a composition of 35.9% C and 1.34% N, giving a molar C:N ratio of 30:1. Measurements in the mesh bags indicated 81.2% (4856 ± 60 mmol) of the original amount had been degraded by day 60 (Tables 1, S1, S2, S3). Loss of C from biomass in the mesh bags over time was best described by a two-component exponential decay model ($R^2 = 0.995$) (Fig. 2), which suggests that kelp degradation was characterised by two pools of OM with different reactivities. Approximately 27% of the total C biomass was lost over the first 3 days (hereafter referred to as the first phase, corresponding to easily leached, reactive OM). The remaining 54.2% (of the total 81.2% used OM) biomass was degraded more slowly (second phase, corresponding to less reactive OM).

Carbon flux estimates (Fig. 3, Tables 1, S2) show that by the end of 60 days of degradation, per mole of *E. radiata* C (where, each g of dry detritus contained 29.89 mol C), 0.48 ± 0.0.34 mol C (59.3%) was converted to $DOC_{Porewater}$ of which 0.25 ± 0.07 mol C (31.8%) was converted to $DIC_{Porewater}$ in porewater. Over the same period 0.03 ± 0.02 mol C (3.2%) and

$4.5\times10^{-5}\pm7.4\times10^{-5}$ mol C (0.006%) were emitted as $CO_{2Emission}$ and $CH_{4Emission,}$ respectively. Of the total used C, carbonate alkalinity 0.27 ± 0.05 mol C (33%) was produced at a depth of 100 cm.

In the ranked permutational ANOSIM, R represents the variability of the parameter (C) that is explained by the variables (time and depth). The results showed that depth ($R=0.35$) had a greater influence on the degradation for the various C components than time ($R=0.25$) (data not shown). Ranking the normalised C-components further with nMDS revealed a depth dependent clustering, where the surface samples (1 cm) were distinct from those in the deeper sediments (Fig. S2) and the deepest sediment was the driver for C-components of the sediments (depths 10–60 cm).

Within sediment processing

Carbon transformations were quickly detected after the first tidal flush (after 4 h) (Fig. 4). Under the degrading wrack, high concentration plumes of $DOC_{Porewater}$ occurred in the first 3 days of the incubation (Fig. 4a), when averaged concentrations near the surface reached 839 ± 557 mmol/L. $DOC_{Porewater}$ concentrations were highest in the first phase, while $DIC_{Porewater}$ concentrations were high only in the second phase and $DIC_{Porewater}$ concentrations increased with depth. The average $DOC_{Porewater}$ concentration (74.9 mmol/L, ranging between 0.1 and 1112 mmol/L) over the 60 days was higher than the $DIC_{Porewater}$ concentration (7.7 mmol/L, ranging between 0.9 and 22.4 mmol/L) (Fig. 4b).

The two phases of degradation were apparent in $CO_{2Porewater}$, with concentrations increasing twice over the 60 days. The first phase of $CO_{2Porewater}$ production peaked on day 6 and the second phase on day 45 (Fig. 5). During the second peak, $CO_{2Porewater}$ concentrations were elevated over a longer period than in the first phase (from day 30 to day 60) (Fig. 4c), but overall, $CO_{2Porewater}$ concentrations ranged between 0.4 and 23 mmol/L. $CH_{4Porewater}$ represented the smallest proportion of C released during the kelp wrack degradation (Table 1, Fig. 3). Further, during the first 10 days, concentrations were below the control level (0.0008 mmol/L) (Fig. 4d). Overall $CH_{4Porewater}$ concentrations ranged between 0.0006 and 0.02 mmol/L, with the highest concentrations measured on days 30 and 45 at a depth of 100 cm (Figs. 4 and 5).

Under the degrading wrack, $DOC_{Porewater}$ and $TA_{Porewater}$ concentrations increased concurrently (Fig. 4e). The two phases were also apparent on $TA_{Porewater}$ production with concentrations highest on days 3 and 45. Overall, $TA_{Porewater}$ concentrations increased with depth and the average concentrations (9.7 mmol/L, ranged between 0.7 and 34.3 mmol/L) were higher than those of $DIC_{Porewater}$ (7.74 mmol/L). At the start of the degradation, $NH_4^+{}_{Porewater}$ concentrations in treatment mesocosms (Fig. 4f) were elevated near the surface (1 and 10 cm depth) and were also high on days 45 and 60, but in the sediment below 30 cm. In the treatment mesocosm, the average $NH_4^+{}_{Porewater}$ concentrations were 1.3 mmol/L and the average $PO_4^{3-}{}_{Porewater}$ concentrations were 1.18 mmol/L. The *t* tests showed that concentrations of all measured components (averaged over time and depth) differed significantly between the control and the treatment mesocosms for $DIC_{Porewater}$, $DOC_{Porewater}$, $TA_{Porewater}$, $NH_4^+{}_{Porewater}$, $PO_4^{3-}{}_{Porewater}$, $CO_{2Porewater}$, $CO_{2Emission}$, $CH_{4Porewater}$, pH and DO, but not for $CH_{4Emission}$ (Table S4).

Discussion

This study highlights the dynamic nature of kelp wrack degradation on sandy beaches and its effect on the quality and quantity of porewater carbon. This study also confirmed that the products of wrack degradation can be transported to the coastal marine environment via porewater flushing and have the potential to impact coastal carbon cycling and storage. Over 60 days of degradation, 200 g (dry weight) *E. radiata* supplied 4865 mmol of C (81% of total the biomass), of which approximately 60% was released into the porewater (at a depth of 100 cm) in the form of $DOC_{Porewater}$ (2880 ± 1992 mmol C) and approximately 31% in the form of $DIC_{Porewater}$ (1514 ± 437 mmol C). Wrack degradation not only supplied high inorganic and organic C to the underlying sediment, as has previously been reported (Van Erk et al. 2020), but also produced alkalinity. Although the release of DOC to porewater represented the largest C processing pathway, the release of alkalinity was significant (1618 ± 158 mmol, 33.3%). Both DOC and alkalinity produced through wrack degradation and remineralisation could represent important, and as yet overlooked, blue carbon

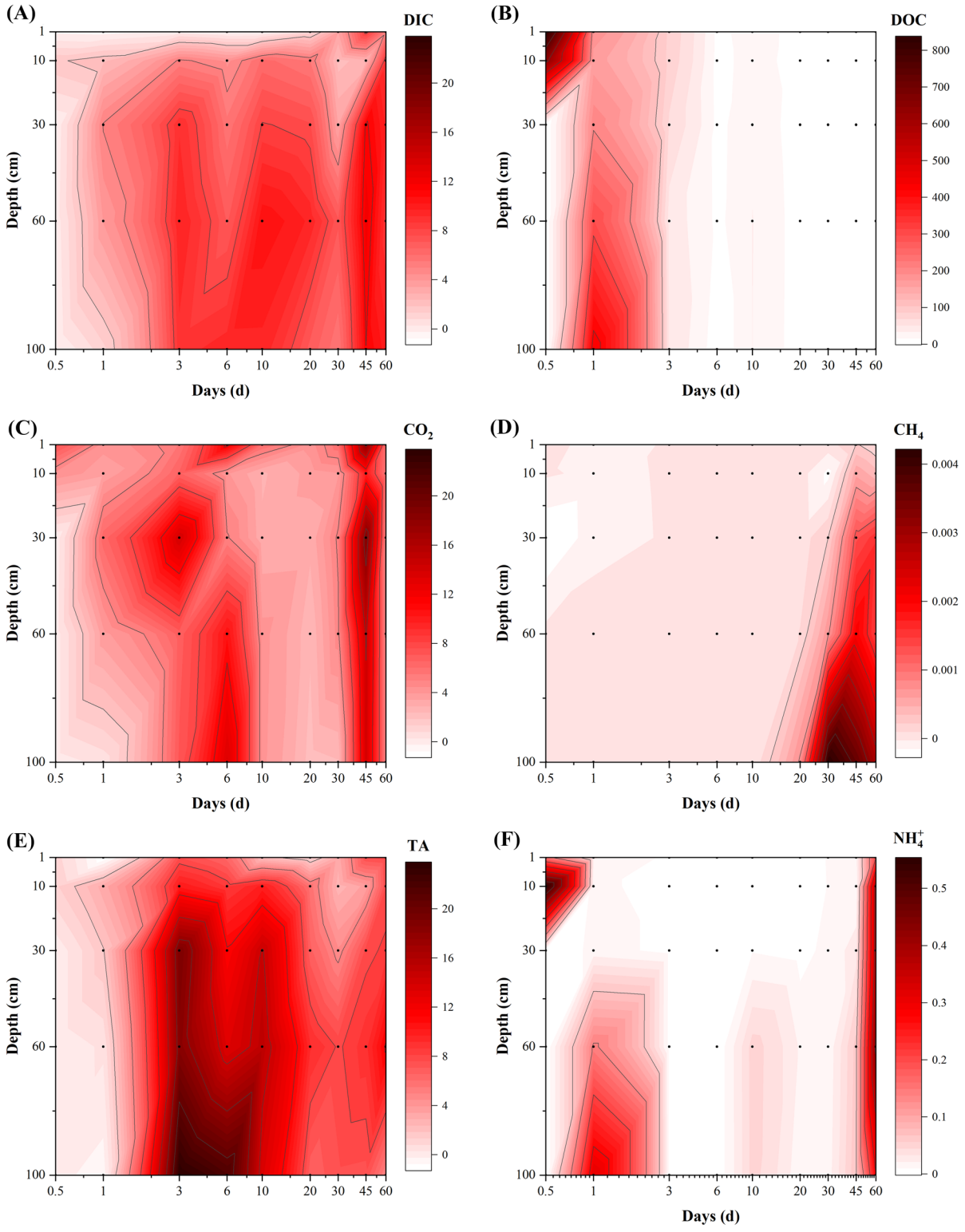
(A)
DIC
(B)
DOC
(C)
CO_2
(D)
CH_4
(E)
TA
(F)
NH_4^+
Depth (cm)
Days (d)
1
10
30
60
100
0.5
1
3
6
10
20
30
45
60
0
4
8
12
16
20
100
200
300
400
500
600
700
800
0.001
0.002
0.003
0.004
0.1
0.2
0.3
0.4
0.5

◂**Fig. 4** *Average changes in* **a** $DiC_{Porewater}$, **b** $DOC_{Porewater}$, **c** $CO_{2Porewater}$, **d** $CH_{4Porewater}$, **e** TA and **f** $NH_4^+{}_{Porewater}$ concentrations in treatment mesocosms relative to controls (treatment concentrations minus control concentrations) at each sediment depth over 60 days (n = 4). All concentrations have units of mmol/L. Black dots indicate time and depth of sample collection points. Please note for DIC (− 0.5–12.1 mmol/L), $CO_{2Porewater}$ (− 0.15–18.8 mmol/L), and TA (− 1.3–23.8 mmol/L) the same scale has been used in the legend for comparison

components (Santos et al. 2021) if at least part of the metabolic products (e.g., reduced Fe and S) are permanently removed (i.e., long-term burial) and the DOC is not remineralised.

The contribution of macroalgae to blue carbon through degradation and remineralisation was assessed via a mass balance. The degradation was initially dominated by a $DOC_{Porewater}$ plume (0.3 ± 0.3 mol C, or 27% of highly reactive OM, as calculated in the decay model Fig. 2) and this labile DOC was quickly remineralised into inorganic C (alkalinity or CO_2). The subsequent production of $DIC_{Porewater}$ (0.25 ± 0.07 mol C) in the second phase showed that the initially released DOC was likely converted into $DIC_{Porewater}$ (Kristensen et al. 1995) at depths of 100 cm. Processing of the DOC can also be observed from the rising $CH_{4Porewater}$ at a depth of 100 cm from day 20 onwards, as the beginning of the second peak. The rising $CH_{4Porewater}$ was followed by the increase of DIC and $CO_{2Emission}$ from day 30 onwards (Figs. 3, 4 and 5). The first phase of degradation produced nearly equal amounts of DIC (0.25 ± 0.07 mol C, or 25%) and TA (0.27 ± 0.03 mol, or 27% of total C assuming TA approaches carbonate alkalinity) that could contribute to blue carbon.

The production of $DOC_{Porewater}$ in the second phase of degradation (0.18 ± 0.04 mol C, or 18% of the total C) is also potentially important for blue carbon, and this production of DOC is in-line with the export of 5–20% of *Sargassum* net community production as refractory DOC (Watanabe et al. 2020). DOC from donor habitats often subsidies the DOC of adjacent receiver habitats. DOC is likely to continue to degrade in these receiver habitats (Sawstrom et al. 2016), but its longevity in the ocean is far from being understood (Baltar et al. 2021). Given that the $DOC_{Porewater}$ from the second phase was not converted to inorganic C, this DOC is likely not very bioavailable, if at all, and could represent a CO_2 sink, if it remains in the coastal ocean for over 150 days (Watanabe et al. 2020). The 33% of *E. radiata* biomass C that was not found in the DOC pool or within the biomass remaining by the end of the 60 days was likely washed away as refractory DOC or fine particulate matter via porewater flow as the mesocosms were drained to emulate an outgoing tide. The portion of wrack that was not degraded over 60 days (0.19 ± 0.01 mol C, or 19%) would most likely ultimately be buried, and therefore represents the contribution of macroalgae to conventional blue carbon storage.

The production of alkalinity from wrack remineralisation is important for coastal C cycling. The average measured TA was four-fold higher (9.5 mmol/L) than that seen in the control (2.3 mmol/L), with the highest measured TA (34.3 mmol/L) being more than 15-fold higher under the degrading kelp wrack. Over 60 days, $TA_{Porewater}$ accounted for 27% of the total C from *E. radiata* biomass assuming TA is made up primarily of bicarbonate. Our mass balance calculations were combined with the biomass of *E. radiata* around Australia (Filbee-Dexter and Wernberg 2020) to estimate the potential for remineralised carbonate alkalinity to contribute blue carbon (Table 2). These calculations assume the same degradation conditions (e.g., sunlight, temperature, or inundation) simulated in our experiment. The alkalinity produced from DOC and from POC, assuming that 60–80% (mean 70%) of macroalgal biomass is removed by grazing before degradation (Griffith and Stenton-Dozey, 1981), could amount to of 0.7–1.55 Tg C yr^{-1}, with remineralisation potential near kelp beds possibly accounting for an additional 1.26–2.78 Tg C yr^{-1} of alkalinity. Although the actual number would be determined if the metabolic products are stored or oxidised, and thus, the available alkalinity could range from between 10 and 100% of these values, depending on the environmental conditions. Notwithstanding this uncertainty, the current study demonstrates that macroalgae have the potential to be significant blue carbon contributors; our estimate for stranded macroalgae, together with macroalgal detritus transported to the deep sea (1.3–2.8 Tg C yr^{-1} Filbee-Dexter and Wernberg (2020)), indicates that macroalgal blue carbon contribution could be on the same order of magnitude as blue carbon burial in broadly recognised blue carbon habitats (i.e., seagrass beds, mangrove forests and salt marshes, contributing blue

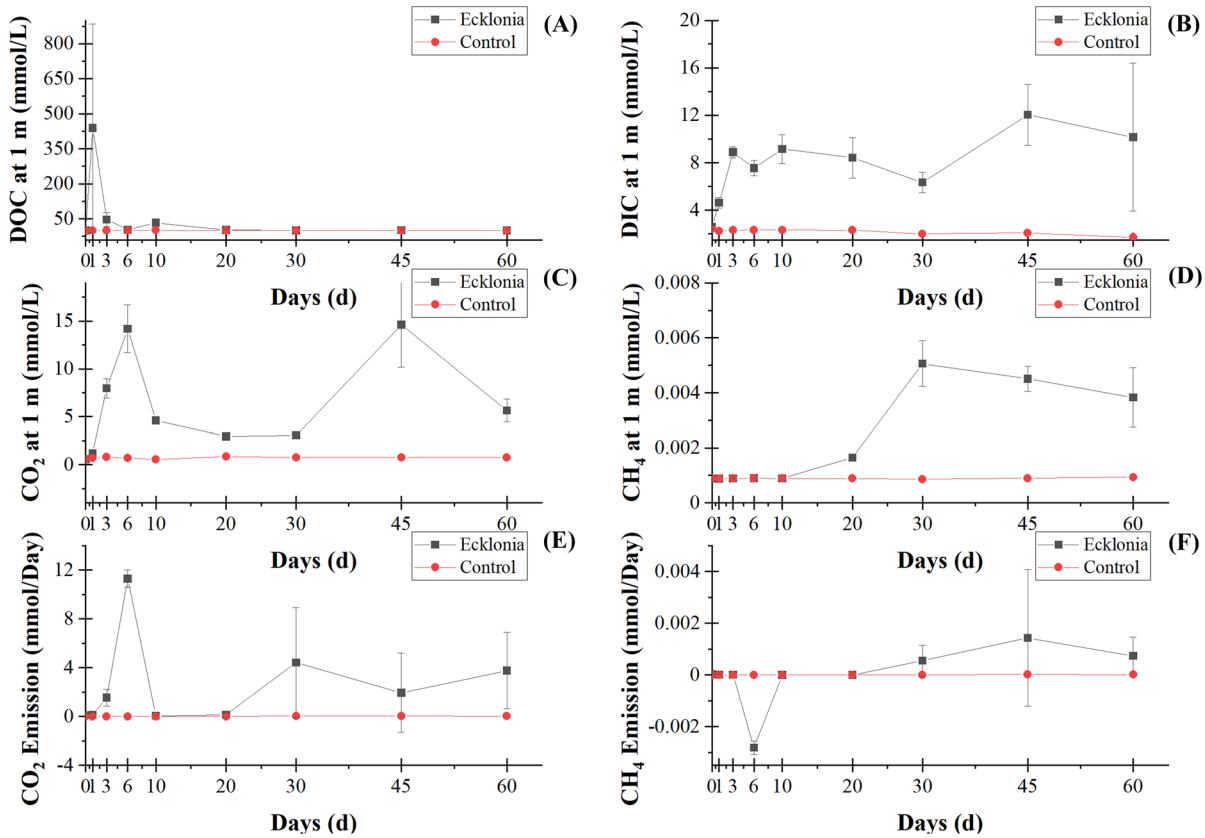

Fig. 5 Time series graphs with averaged concentrations (±standard error) at 100 cm sediment depth

carbon of 3.5–5.5 Tg C yr^{-1}) (Filbee-Dexter and Wernberg 2020).

Stoichiometric TA:DIC ratios can be used to understand the biogeochemical mechanisms underlying alkalinity production (e.g. aerobic respiration, denitrification, ammonification, sulphate reduction, calcium carbonate dissolution, manganese reduction, and iron reduction) (Borges et al. 2003). TA:DIC ratios in the first phase (days 0–3) of this study were comparable to those produced during calcium carbonate dissolution (Fig. 6a). For the second decomposition phase, the TA:DIC ratio suggested that the decomposition was instead mainly driven by coupled ammonification and sulphate reduction (Fig. 6b). This is in line with a previous study; Van Erk et al. (2020) also found that sulphate reduction was the driver for kelp degradation on a beach (high sulphide levels > 10 mmol/L). The sulphur content of seawater is high (28 mg kg^{-1}) and in the macroalgae it can range from 2.9 to 57.5 g kg^{-1} of dry weight (Machado et al. 2015). Kelp deposition on beaches has been found to increase the sulphate reduction rate by 20- to 25-fold (Van Erk et al. 2020) with sulphur concentrations decreasing during degradation (King et al. 1985). The reduced sulphate can be released to the surrounding sediments, porewater, and to seawater. Sulphate reduction is part of anaerobic C mineralisation and is important for alkalinity production.

Sulphate reduction and ammonification are the main pathways for kelp degradation, and both generate high TA values (Berner et al. 1970; Ferguson et al. 2003; Hu and Cai 2011). Sulphate reduction releases 1.98 mol of alkalinity per mol SO_4^{2-}, while denitrification releases 0.99 mol of alkalinity per denitrified mol N, and net ammonification (ammonification – nitrification) also generates alkalinity (Krumins et al. 2013). Sulphate reduction can account for a large portion of the organic C oxidised on the continental shelf and deeper sediments. For example, Krumins et al. (2013) reported that sulphate reduction

Table 2 The potential contribution of *E. radiata* to alkalinity production and carbon sequestration through degradation and remineralisation, assuming minimum and maximum removal of kelp biomass through grazing and a range of 10–100% of the alkalinity be available

Potential remineralisation pathways	NPP sequestered ± SD Mg C ha^{-1} yr^{-1}	NPP alkalinity ± SD Mg C ha^{-1} yr^{-1}	Sequestration rates Tg C yr^{-1}
DOC export	0.61 ± 0.14	0.16 ± 0.04	0.53–1.16
Total POC export	0.66 ± 0.15	0.18 ± 0.04	0.58–1.27
POC export excluding buried + grazed min	0.26 ± 0.06	0.07 ± 0.02	0.23–0.51
POC export excluding buried + grazed max	0.13 ± 0.03	0.04 ± 0.01	0.12–0.25
Remineralised near kelp beds	1.45 ± 0.33	0.39 ± 0.09	1.26–2.78
Total sum			1.97–4.33

Total carbon production was estimated by above ground biomass net primary production (NPP), and sequestration rates were determined by multiplying NPP values by the estimated area coverage of *E. radiata* in Australian waters (Filbee-Dexter amd Wernberg 2020). The alkalinity production was estimated from the mass balance (27%)

[a]For this calculation we assumed the total area coverage of *E. radiata* in Australia (eastern, southern and western region) to be 3.2–7.1 Mha with a total biomass ca. 10.3–22.7 Tg C and the total NPP 3.86 ± 0.87 Mg C ha^{-1} yr^{-1} (as estimated by Filbee-Dexter and Wernberg 2020)

[b]The total carbon production was estimated using the global macroalgal NPP calculated by Krause-Jensen and Duarte (2016) to be 1521 Tg C yr^{-1}, of which a min 37.3% is remineralised near kelp beds (567 Tg C yr^{-1}), with 15.6% (238 Tg C yr^{-1}) converted to DOC, and 274 Tg C yr^{-1} converted to POC of which 14 Tg C yr^{-1} is buried in sediments, equals to 17.1% (260 Tg C yr^{-1})

[c]A portion of POC was assumed to be removed via grazing, based on an estimate that 60–80% (mean 70%) of kelp biomass is grazed over 14 days (Griffith and Stenton-Dozey 1981). After accounting for the minimum grazed (60%), 6.8% of the total biomass (104 Tg C yr^{-1}) is exported as POC, and accounting for the maximum grazed (80%), 3.4% of the total biomass (52 Tg C yr^{-1}) is exported as POC with the mean amount grazed (70%) seeing 5.1% (78 Tg C yr^{-1}) of POC being remineralised and exported. The assumed removal of biomass via grazing likely leads to an underestimate of alkalinity production; grazing would not lead to immediate removal of biomass, but rather its gradual removal over 14 days, during which time the highly reactive portion of *E. radiata* would release some alkalinity

[d]Total Sum is represented by the sum of remineralised biomass: (1) near kelp beds, being 37.3%, (2) as DOC, being 15.6% and (3) as POC, being 5.1% [excluding buried and the grazed mean (value midway between min and max)]. These values result in the total sum of 58% of NPP for the potential for blue carbon, from remineralisation to alkalinity

accounted for 85% to 150 m depth and 77% at 150 m depth of organic C oxidation around the continental shelf sediments. As a recognised significant biological alkalinity source, anaerobic degradation via sulphate reduction has the capacity to absorb atmospheric CO_2 and counteract rising CO_2 emissions (Chen and Wang, 1999; Thomas et al. 2009; Liu et al. 2021).

The elevated production of $TA_{Porewater}$ and $DIC_{Porewater}$ in the deeper sediments (Figs. 4 and 5) coincided with higher pH and lower DO concentrations (Fig S1). This indicates that DO and pH were uncoupled during decomposition. This is likely because the organic acids leaching out of the kelp first lower the pH and shift the carbonate equilibrium. However, the release of organic acids in contact with seawater and the TA production from sulphate reduction reduces the available O_2 but favours calcium carbonate dissolution, which in turn raises the pH (James and Bone 2011; Reid et al. 2011). The oxidant concentration for sulphate reduction has been reported as 28 mM, using the approximate concentrations in seawater (Santos et al. 2021). Therefore, the amount of O_2 available during anaerobic mineralisation (ammonification and sulphate reduction) determines the amount of C being processed (Torres et al. 2017).

Kelp C may contribute to blue carbon in various ways but C transportation is important for delivering TA or DIC and in determining how C can influence the adjacent ocean. C products from wrack degradation and remineralisation can be considered as 'mobile carbon' (Santos et al. 2021) that is redistributed with tides, currents and via porewater transport to the ocean. Small organic particles resulting from wrack fragmentation during decay, or medium molecular weight compounds produced during degradation, are transported downwards into deeper sediment or into porewater. The extent of downward transport in

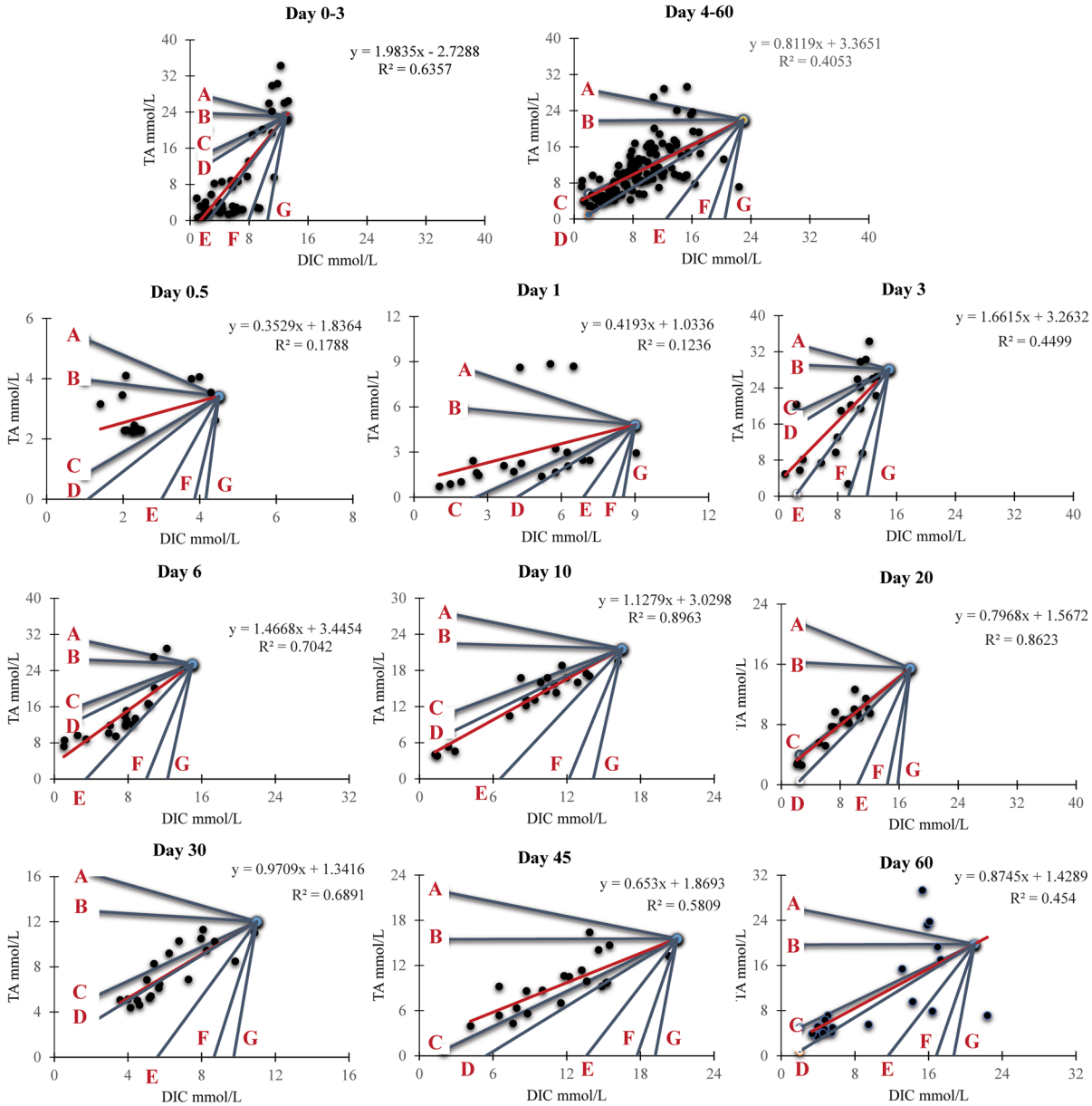

Fig. 6 Correlation of TA:DIC (concentration in treatment only) during **A** the first phase of degradation (easily leached, reactive OM during days 0–3), **B** the second phase degradation (less reactive OM during days 4–60) and **C**–**K** each of the sampling days. The red line indicates the trend line and the other lines indicate the stoichiometric relationships between TA and DIC expected from (A) aerobic respiration, (B) nitrification, (C) ammonification, (D) sulphate reduction, (E) calcium carbonate dissolution, (F) manganese and (G) iron reduction

the environment will vary temporally and spatially, but downward transport may explain why depth was a more important factor than time in determining kelp degradation pathways (Fig. S2). The remineralised products from a depth of 100 cm in the sediment can re-enter the marine environment via tidal driven porewater advection to a 'receiver' habitat, where they can influence C cycling or storage. Queirós et al. (2019) described the connectivity between individual ocean components, transporting macroalgal C from

macroalgal beds to other habitats. The transportation however, is governed by several factors (e.g., permeability of the sand, tidal forces, density-driven convection, wave pumping, topography and temperature) (Santos et al. 2012). Here, we assumed that all material at a depth of 100 cm was transported, but further studies would be required to determine the extent of kelp remineralisation into DOC, DIC and TA, how much of the TA remains after sulphide oxidation (e.g., reduced Fe and S are permanently removed by long-term burial) and how porewater transports these C products to other systems. In the natural environment this would be challenging to investigate due to the high variability of kelp deposition, environmental conditions, multi-dimensional pathways and the relevant redox cycling. Mesocosm experiments provide an effective alternative approach to exploring the underlying biogeochemical pathways of macroalgae degradation.

Conclusions

We report wrack degradation experiments simulating the tidal zone of a sandy beach. This study demonstrates that labile, leached carbon first enters the porewater primarily as DOC. The highly reactive OM is later converted into DIC and alkalinity. The carbonate alkalinity generated during kelp degradation through sulphate reduction is a major pathway for anaerobic microbial respiration in the ocean and marine sediments as well as an important contributor to carbon sequestration if at least part of the metabolic products (e.g., reduced Fe and S) are permanently removed (i.e., long-term burial). This study indicated that 33.3% of kelp biomass deposited on a sandy beach can be converted into alkalinity via sulphate reduction. Given that this sulphate reduction was likely driven by macroalgal degradation, it is reasonable that remineralisation of macroalgae in subtidal habitats also generates alkalinity. Despite the uncertainties of our calculations, they provide evidence that alkalinity production from macroalgae degradation and remineralisation has the potential to be a significant blue carbon process. Wrack degradation may also contribute to blue carbon sequestration via conversion of 18.3% of the macroalgal biomass into semi-labile or refractory DOC. Considering the high productivity of macroalgal habitats, and the large quantities of detritus they produce, this study indicates that blue carbon budgets for marine systems on a global scale will only be complete with the inclusion of macroalgae. Further studies on the decomposing microbiota of kelp would greatly enhance our understanding of marine C cycling for blue carbon processes.

Acknowledgements We thank Dr Bennan Chen and James Tucker for their assistance with building the mesocosms and Ceylena Holloway, Matheus Carvalho de Carvalho, Iain Alexander and Natasha Carlson-Perret for their laboratory support.

Author contributions AKP, IRS, BK conceived the project and designed methodology. AKP collected the samples, analysed the data and led the writing of the manuscript. IRS, JMO, ALR, BDE, KGS, HPG assisted with data interpretation. All authors contributed critically to improve the drafts and approved the final version for publication.

Funding Open Access funding enabled and organized by Projekt DEAL. The authors have no relevant financial or non-financial interests to disclose.

Data availability All data relevant is in Supplementary Information.

Code availability Not applicable.

Declarations

Conflict of interest The authors have no conflict of interest to declare that are relevant to the content of this article.

Ethical approval This project required a scientific licence from the NSW Government, Office of Environment & Heritage, NSW National Parks & Wildlife Service (licence number SL101847, valid from 20/01/2017 to 31/12/2019). The licence authorised the collection of samples (soil, water and *Ecklonia radiata*) on NPWS estate for research purposes.

References

Alongi DM (2020) Carbon balance in salt marsh and mangrove ecosystems: a global synthesis. J Mar Sci Eng 8(10):767. https://doi.org/10.3390/jmse8100767

Baltar F, Alvarez-Salgado XA, Aristegui J, Benner R, Hansell DA, Herndl GJ, Lonborg C (2021) What is refractory organic matter in the ocean? Front Mar Sci 8:642637. https://doi.org/10.3389/fmars.2021.642637

Berner RA, Scott MR, Thomlinson C (1970) Carbonate alkalinity in the pore waters of anoxic marine sediments. Limnol Oceanogr 15(4):544–549. https://doi.org/10.4319/lo.1970.15.4.0544

Borges AV, Djenidi S, Lacroix G, Théate J, Delille B, Frankignoulle M (2003) Atmospheric CO_2 flux from mangrove surrounding waters. Geophys Res Lett 30:11. https://doi.org/10.1029/2003GL017143

Chen C-TA, Wang SL (1999) Carbon, alkalinity and nutrient budgets on the east China sea continental shelf. J Geophys Res Oceans. 104(C9):20675–20686. https://doi.org/10.1029/1999jc900055

Dickson AG, Afghan JD, Anderson GC (2003) Reference materials for oceanic CO_2 analysis: a method for the certification of total alkalinity. Mar Chem 80(2–3):185–197. https://doi.org/10.1016/S0304-4203(02)00133-0

Duarte CM (2017) Reviews and syntheses: hidden forests, the role of vegetated coastal habitats in the ocean carbon budget. Biogeosciences 14:301–310. https://doi.org/10.5194/bg-14-301-2017

Ferguson AJP, Eyre BD, Gay JM (2003) Organic matter and benthic metabolism in euphotic sediments along shallow sub-tropical estuaries, northern new South Wales Australia. Aquat Microb Ecol 33(2):137–154. https://doi.org/10.3354/ame033137

Filbee-Dexter K, Wernberg T (2020) Substantial blue carbon in overlooked Australian kelp forests. Sci Rep 10:12341. https://doi.org/10.1038/s41598-020-69258-7

Gattuso J-P, Gentili B, Duarte CM, Kleypas JA, Middelburg JJ, Antoine D (2006) Light availability in the coastal ocean: impact on the distribution of benthic photosynthetic organisms and their contribution to primary production. Biogeosciences 3:489–513. https://doi.org/10.5194/bg-3-489-2006

Griffiths CL, Stenton-Dozey J (1981) The fauna and rate of degradation of stranded kelp. Estuar Coast Shelf Sci 12(6):645–653. https://doi.org/10.1016/S0302-3524(81)80062-X

Hill R, Bellgrove A, Macreadie PI, Petrou K, Beardall J, Steven A, Ralph PJ (2015) Can macroalgae contribute to blue carbon? An Australian perspective. Limnol Oceanogr 60(5):1689–1706. https://doi.org/10.1002/lno.10128

Hu X, Cai WJ (2011) An assessment of ocean margin anaerobic processes on oceanicalkalinity budget. Glob Biogeochem Cycles 25:3. https://doi.org/10.1029/2010GB003859

James NP, Bone Y (2011) Carbonate production and deposition in a warm-temperate macroalgal environment, investigator strait South Australia. Sedim Geol 240(1–2):41–53. https://doi.org/10.1016/j.sedgeo.2011.07.005

Jones DL, Willett VB (2006) Experimental evaluation of methods to quantify dissolved organic nitrogen (DON) and dissolved organic carbon (DOC) in soil. Soil Biol Biochem 38(5):991–999. https://doi.org/10.1016/j.soilbio.2005.08.012

Kelaher BP, Bishop MJ, Potts J, Scanes P, Skilbeck G (2013) Detrital diversity influences estuarine ecosystem performance. Glob Change Biol 19:1909–1918. https://doi.org/10.1111/gcb.12162

Kelleway J Serrano O Baldock J et al. (2017) Technical review of opportunities for including blue carbon in the Australian Government's Emissions Reduction Fund. Final Report. Prepared for the Department of the Environment and Energy. https://publications.csiro.au/rpr/download?pid=csiro:EP166570&dsid=DS2 Accessed 25 Aug 2021

King GM, Guist GG, Lauterbach GE (1985) Anaerobic degradation of carrageenan from the red macroalga *Eucheuma cottonii*. Appl Environ Microbiol 49(3):588–592. https://doi.org/10.1128/AEM.49.3.588-592.1985

Kirkman H, Kendrick GA (1997) Ecological significance and commercial harvesting of drifting and beach-cast macroalgae and seagrasses in Australia: a review. J Appl Phycol 9:311–326. https://doi.org/10.1023/A:1007965506873

Krause-Jensen D, Duarte CM (2016) Substantial role of macroalgae in marine carbon sequestration. Nat Geosci 9(10):737–742. https://doi.org/10.1038/ngeo2790

Krause-Jensen D, Lavery P, Serrano O, Marbá N, Masque P, Duarte CM (2018) Sequestration of macroalgal carbon: the elephant in the blue carbon room. Biol Lett 14:20180236. https://doi.org/10.1098/rsbl.2018.0236

Kristensen E, Ahmed SI, Devol AH (1995) Aerobic and anaerobic decomposition of organic matter in marine sediment: which is fastest? Limnol Oceanogr 40(8):1430–1437. https://doi.org/10.4319/lo.1995.40.8.1430

Krumhansl KA, Scheibling RE (2012) Production and fate of kelp detritus. Mar Ecol Prog Ser 467:281–302. https://doi.org/10.3354/meps09940

Krumins V, Gehlen M, Arndt S, Van Cappellen P, Regnier P (2013) Dissolved inorganic carbon and alkalinity fluxes from coastal marine sediments: model estimates for different shelf environments and sensitivity to global change. Biogeosciences 10:371–398. https://doi.org/10.5194/bg-10-371-2013

Lechtenfeld OJ, Kattner G, Flerus R, McCallister LS, Schmitt-Kopplin P, Koch BP (2014) Molecular transformation and degradation of refractory dissolved organic matter in the Atlantic and southern ocean. Geochim Cosmochim Acta 126:321–337. https://doi.org/10.1016/j.gca.2013.11.009

Liu Y, Jiao JJ, Liang W, Santos IR, Kuang X, Robinson CE (2021) Inorganic carbon and alkalinity biogeochemistry and fluxes in an intertidal beach aquifer: implications for ocean acidification. J Hydrol 595:126036. https://doi.org/10.1016/J.JHYDROL.2021.126036

MacCharthy GR (1933) Calcium carbonate in beach sands. J Sediment Petrol 3(2):64–67

Machado L, Kinley RD, Magnusson M, De Nys R, Tomkins NW (2014) The potential of macroalgae for beef production systems in northern Australia. J Appl Phycol 27:2001–2005. https://doi.org/10.1007/S10811-014-0439-7

Macreadie PI, Anton A, Raven et al (2019) The future of blue carbon science. Nat Commun 10(1):3998. https://doi.org/10.1038/s41467-019-11693-w

Maher DT, Santos IR, Leuven JRFW, Oakes JM, Erler DV, Carvalho MC, Eyre BD (2013) Novel use of cavity ring-down spectroscopy to investigate aquatic carbon cycling from microbial to ecosystem scales. Environ Sci Technol 47(22):12938–12945. https://doi.org/10.1021/es4027776

Marzinelli EM, Williams SB, Babcock RC et al (2015) Large-scale geographic variation in distribution and abundance of Australian deep-water kelp forests. PLoS ONE 10(2):e0118390. https://doi.org/10.1371/journal.pone.0118390

McKee L, Eyre BD, Hossain S (2000) Intra- and inter-annual export of nitrogen and phosphorus in the sub-tropical richmond river catchment Australia. Hydrol Process. 14(10):1787–1809

McLeod E, Chmura GL, Bouillon et al (2011) A blueprint for blue carbon: toward an improved understanding of the role of vegetated coastal habitats in sequestering CO_2. Front Ecol Environ 9(10):552–560. https://doi.org/10.1890/110004

Mos B, Holloway C, Kelaher BP, Santos IR, Dworjanyn SA (2021) Alkalinity of diverse water samples can be altered by mercury preservation and borosilicate vial storage. Sci Rep 11(1):9961. https://doi.org/10.1038/s41598-021-89110-w

Queirós AM, Stephens N, Widdicombe S et al (2019) Connected macroalgal-sediment systems: blue carbon and food webs in the deep coastal ocean. Ecol Monogr. 89(3):e01366. https://doi.org/10.1002/ecm.1366

Raven J (2018) Blue carbon: past, present and future, with emphasis on macroalgae. Biol Lett 14:20180336. https://doi.org/10.1098/rsbl.2018.0336

Reid CM, James NP, Bone Y (2011) Carbonate sediments in a cool-water macroalgal environment, Kaikoura New Zealand. Sedimentology 58(7):1935–1952. https://doi.org/10.1111/j.1365-3091.2011.01246.x

Rosentreter JA, Maher DT, Erler DV, Murray RH, Eyre BD (2018) Methane emissions partially offset "blue carbon" burial in mangroves. Sci Adv. https://doi.org/10.1126/sciadv.aao4985

Saderne V, Fusi M, Thomson T et al (2020) Total alkalinity production in a mangrove ecosystem reveals an overlooked blue carbon component. Limnol Oceanogr Lett 6:61–67. https://doi.org/10.1002/lol2.10170

Santos IR, Eyre BD, Huettel M (2012) The driving forces of porewater and groundwater flow in permeable coastal sediments: a review. Estuar Coast Shelf Sci 98:1–15. https://doi.org/10.1016/J.ECSS.2011.10.024

Santos IR, Burdige DJ, Jennerjahn TC et al (2021) The renaissance of odum's outwelling hypothesis in "blue carbon" science. Estuar Coast Shelf Sci 255:107361. https://doi.org/10.1016/j.ecss.2021.107361

Säwström C, Hyndes GA, Eyre BD et al (2016) Coastal connectivity and spatial subsidy from a microbial perspective. Ecol Evol 6(18):6662–6671. https://doi.org/10.1002/ece3.2408

Serrano O, Lovelock CE, Atwood TB (2019) Australian vegetated coastal ecosystems as global hotspots for climate change mitigation. Nat Commun. https://doi.org/10.1038/s41467-019-12176-8

Sippo JZ, Maher DT, Tait DR, Holloway C, Santos IR (2016) Are mangroves drivers or buffers of coastal acidification? Insights from alkalinity and dissolved inorganic carbon export estimates across a latitudinal transect. Glob Biogeochem Cycles 30:753–766. https://doi.org/10.1002/2015GB005324

Somerfield P, Clarke K, Gorley R (2021) Analysis of similarities (ANOSIM) for 3-way designs. Aust Ecol. https://doi.org/10.1111/aec.13083

Thomas H, Schiettecatte LS, Suykens, et al (2009) Enhanced ocean carbon storage from anaerobic alkalinity generation in coastal sediments. Biogeosciences 6(2):267–274. https://doi.org/10.5194/bg-6-267-2009

Torres MA, Moosdorf N, Hartmann J, Adkins JF, West AJ (2017) Glacial weathering, sulfide oxidation, and global carbon cycle feedbacks. Proc Natl Acad Sci USA 114(33):8716–8721. https://doi.org/10.1073/pnas.1702953114

Van Erk MR, Meier DV, Ferdelman T, Harder J, Bussmann I, De Beer D (2020) Kelp deposition changes mineralization pathways and microbial communities in a sandy beach. Limnol Oceanogr 65(12):3066–3084. https://doi.org/10.1002/lno.11574

Wagner S, Schubotz F, Kaiser et al (2020) Soothsaying DOM: a current perspective on the future of oceanic dissolved organic carbon. Front Mar Sci 7:341. https://doi.org/10.3389/fmars.2020.00341

Watanabe K, Yoshida G, Hori M, Umezawa Y, Moki H, Kuwae T (2020) Macroalgal metabolism and lateral carbon flows can create significant carbon sinks. Biogeosciences 17:2425–2440. https://doi.org/10.5194/bg-17-2425-2020

Wernberg T, Coleman M, Fairhead A, Miller S, Thomsen M (2003) Morphology of *Ecklonia radiata* (phaeophyta: laminarales) along its geographic distribution in south-western Australia and Australasia. Mar Biol 143:47–55. https://doi.org/10.1007/s00227-003-1069-9